



ORIGINAL ARTICLE

Green synthesis and characterization of terbium orthoferrite nanoparticles decorated with $g\text{-C}_3\text{N}_4$ for antiproliferative activity against human cancer cell lines (Glioblastoma, and Neuroblastoma)



Mahin Baladi ^a, Mahnaz Amiri ^{b,**}, Maryam Amirinezhad ^b,
Waleed K. Abdulsahib ^c, Fatemeh Pishgouii ^b, Zahra Golshani ^d,
Masoud Salavati-Niasari ^{a,*}

^a Institute of Nano Science and Nano Technology, University of Kashan, Kashan 87317-51167, Iran

^b Neuroscience Research Center, Institute of Neuropharmacology, Kerman University of Medical Sciences, 76175-113 Kerman, Iran

^c Department of Pharmacology and Toxicology, College of Pharmacy, Al-Farahidi University, Baghdad, Iraq

^d Department of Chemistry, Shahid Bahonar University of Kerman, P.O. Box 76169-14111, Kerman, Iran

Received 20 October 2022; accepted 20 March 2023

Available online 23 March 2023

KEYWORDS

Cancer Cell Lines;
Cytotoxicity;
Green Synthesis;
TbFeO₃/g-C₃N₄ Nanocomposite;
Nanostructures

Abstract Accordingly, employing plant extracts for the green synthesis of different nanoparticles (NPs) has caught the interest of scientists, and researchers due to the ease of accessibility, widespread distribution, and safety of plants. In the current study, a TbFeO₃/g-C₃N₄ nanocomposite was made using a green chemistry technique that utilized grape juice, which acts as an active capping, and reducing agent to create NPs with well-organized biological characteristics. Several methods, including HRTEM, TEM, SEM, XRD, BET-BJH, and VSM, were employed to characterize the produced NPs. The XRD results indicated that the produced NPs had particles with an average size of 38.74 ± 2 nm, which the TEM examination verified. Additionally, the cytotoxicity of the NPs was examined to assess their anti-proliferative effects on the cancer cell lines T98, and

* Corresponding author.

** Corresponding author.

E-mail addresses: ma.amiri@kmu.ac.ir (M. Amiri), Salavati@Kashanu.ac.ir (M. Salavati-Niasari).

Peer review under responsibility of King Saud University.



SH-SY5. In the case of T98 cells, viability was about 60, 70 and 90% in concentration C1 to C4 respectively after 24 h of drug administration. And viability decreasing by pass the time. Also, viability reduce about 65% in all concentration about SH-SY5Y cells, surprisingly only the first three concentrations, C1 to C3 caused cell death after 48 h of drug administration and in lower concentrations, the death rate should decrease with the passage of time, viability was about 80 and 85% in C4 and C5 respectively.

© 2023 The Author(s). Published by Elsevier B.V. on behalf of King Saud University. This is an open access article under the CC BY license (<http://creativecommons.org/licenses/by/4.0/>).

1. Introduction

In developed nations today, cancer is the leading cause of mortality due to its prevalence as an extremely hazardous disease (Lokapur et al., 2022). So researchers are looking for ways to improve, and treat this disease. Meanwhile, chemotherapy, and other conventional cancer treatment approaches, such as radiation, have substantial disadvantages. High-energy radiation used in radiotherapy inhibits cancer cells, but it is difficult to manage how deeply the radiation penetrates the body (Qi et al., 2015; Yu et al., 2019). Chemotherapy uses chemicals to kill cancer cells, although doing so can have negative side effects, be poisonous, or even harm healthy cells (Grossman and McNeil, 2012). Despite the extensive research efforts, 25% of all fatalities in developed nations are still caused by cancer (Torre et al., 2012; Goudarzi et al., 2019). Therefore, there is a critical need for more accurate, efficient, and sensitive techniques of cancer detection, and treatment. For this reason the use of nanostructures to fight cancer has received much attention.

Nanotechnology is the widespread scientific phenomenon that has spread throughout the scientific community, that is currently advancing as possible (Narducci, 2007). Many changes in the chemical characteristics, morphological, structural, magnetic, and electrical of nanoparticles will occur when their size is optimized (Amiri and Mahmoudi-Moghaddam, 2021). Nanoparticles can be used in a variety of biological, and biomedical applications because of their variable shape, size, structure, and chemical surface characteristics (Ling et al., 2014; Yang et al., 2019). Therefore, nanomaterials as nanocarriers for drugs have represented a unique impact on the treatment of cancer due to their unique interactions with biological systems, such as long circulation times, greater solubility in water, which lowers the rate of cytotoxicity, ease of penetration into the membrane, and their similarity in size to biological structures (Shamim et al., 2021).

Additionally, pharmacokinetic modifications improve therapeutic outcomes by increasing the concentration of the therapeutic agent in cancerous cells (Ordás et al., 2012; Kudarha and Sawant, 2017). Contrary to previous researches, today the effect of the drug in a specific place is of particular interest (Rezaeifar et al., 2016), targeting the drug to a specific site, and maintaining the drug's concentration at that site for the necessary amount of time to produce better effects (Abdulhusain et al., 2022; Mahde et al., 2022).

With their remarkable electromagnetic thermal, and optical capabilities, inorganic nanoparticles, and nanoparticle-biomaterial composites have shown significant promise in innovative approaches for detection, characterization, and cancer treatment (Montaseri et al., 2020). Targeting cancer cells is one of the most crucial aspects of nanoscale-designed materials. A variety of nanomaterials have been created for the detection, and therapy of illnesses, including cancer. Because of their high surface-to-volume ratio, some inorganic nanoparticles exhibit antibacterial qualities, are tiny, and have strong penetration into microorganisms (Huang et al., 2012). Also, their ability to photocatalyze, ionize, and catalyze led to their widespread usage in the fight against human disease microbes, including viruses, bacteria, and fungus. (Wang, 2004; Ashrafuzzaman and Tuszyński, 2012). Magnetite nanoparticles (MNPs)

are potential targeted materials in the biomedical area, and have uses in magnetic hyperthermia, magnetic resonance imaging (MRI), and drug delivery systems (Amiri et al., 2021).

Numerous researchers have examined perovskite nanostructures with the formula ABO_3 because to their distinctive properties, which include superior electrical insulation, low thermal expansion, high chemical stability, high thermal conductivity, and high melting point (Goel et al., 2021).

Due to their inertness, low toxicity, excellent stability, low density, and ease of production, perovskite-type ferrite oxides, like $LnFeO_3$ ($Ln = Nd, Gd, Dy, Y, Sm, La, etc.$), are frequently used as optical switches, isolators, gas sensors, and for enhancing lithium-ion batteries, and magnetic materials (Li et al., 2021; Andrei et al., 2020). Perovskite compounds are created using a variety of conditions, and processes, including pechini, hydrothermal, solid state, ball mill procedure, combustion method, Co-precipitation (Al Alwany, 2022; Majid et al., 2005; Liu et al., 2022; Abdtawfeeq et al., 2022; Maurya et al., 2009; Bobinov et al., 2021; Varandili et al., 2018).

Although $LnFeO_3$ materials are employed in many different sectors, including sensors, photocatalysts, and antibacterials, there hasn't been much antibacterial research on these nanostructures. For example, $LaCoO_3$, $LaFeO_3$, and $LaNiO_3$ nanoparticles have been used as catalysts to kill bacteria (Ye et al., 2020; Guo et al., 2020; Chen et al., 2022).

Also carbon-based nanomaterials, as a drug carrier, due to their specific surface functionalization for diagnostic imaging, minimal cytotoxicity, and capacity to target cancer cells, have recently demonstrated effective promise in the treatment of cancer (Zhang et al., 2006; Yadav and Mohite, 2020).

Recently, among all carbon-nitride allotropes, including the α , β -phase, and structures resembling graphite, researchers have focused on $g-C_3N_4$ (graphitic carbon-nitride), two-dimensional conjugated polymer, metal-free, earth-abundant, a low-cost (Wang et al., 2017), because of its improved efficiency in semi-conductivity, degradation, and sensing applications. It also has a 2.7 eV (bandgap), and higher stability even at room temperature (Zhang et al., 2018; Fei et al., 2018; Liu et al., 2020; Zheng et al., 2021; Chen et al., 2017) compared to the bulk form of $g-C_3N_4$, the ultrathin nanosheets of this compound showed reduced toxicity, improved water solubility, higher biocompatibility, and much higher photoluminescence yields (Farooq et al., 2021). Therefore, it is readily metabolized in biological systems (Zhao et al., 2015; Zhang et al., 2013). The $g-C_3N_4$ is a preferred material for biomedical applications, particularly in the field of cancer therapy, due to its high biocompatibility, and low biotoxicity (Dai et al., 2019). Additionally, $g-C_3N_4$ shares structural similarities with graphene, but because of its better characteristics, it has drawn a lot of interest (Wang et al., 2012).

In general, there are different physical, chemical and biological methods for preparing nanoparticles, but the methods that require lower temperature (in the range of ambient temperature), less covering materials, less organic solvent, require simpler and more economical facilities, are environmentally friendly methods and receive more attention. Among these, green chemistry methods or biological meth-

ods are of particular importance. In these methods, one or more natural agents in nature are usually used for the synthesis of nanoparticles. grape (*Vitis vinifera*), one of the most widely consumed fruit worldwide; contains many bioactive constituents including flavonoids, polyphenols, anthocyanins and stilbene derivatives resveratrol. The components present in grape juices have been reported for anticarcinogenic, antimutagenic, antiangiogenic, antioxidant, antibacterial and antiviral properties and also have broad-range of applications in pharmaceuticals, medical, cosmetic and food industry. Also, due to the presence of significant amounts of sugars and organic acids, it can be used as a natural and available fuel for the synthesis of nanoparticles (Zia et al., 2017; Hussein and Mohammed, 2021).

In the current study, TbFeO_3 nanoparticles were synthesized using green chemistry method in the presence of grape extract. the fabrication of $\text{TbFeO}_3/\text{g-C}_3\text{N}_4$ using mechanical mixing, and ultrasonic techniques was described. Throughout the fabrication process, TbFeO_3 nanoparticles made using the sol-gel technique, and then loaded onto $\text{g-C}_3\text{N}_4$ layered nanosheets to produce a variety of products with a range of doping ratios. Lastly, the anti-cancer activity of synthesized nanocomposite on two different cell lines (T98 and SH-SY5Y) investigated. Based on our research, it is the first time that anticancer ability of $\text{TbFeO}_3/\text{g-C}_3\text{N}_4$ nanocomposite presented.

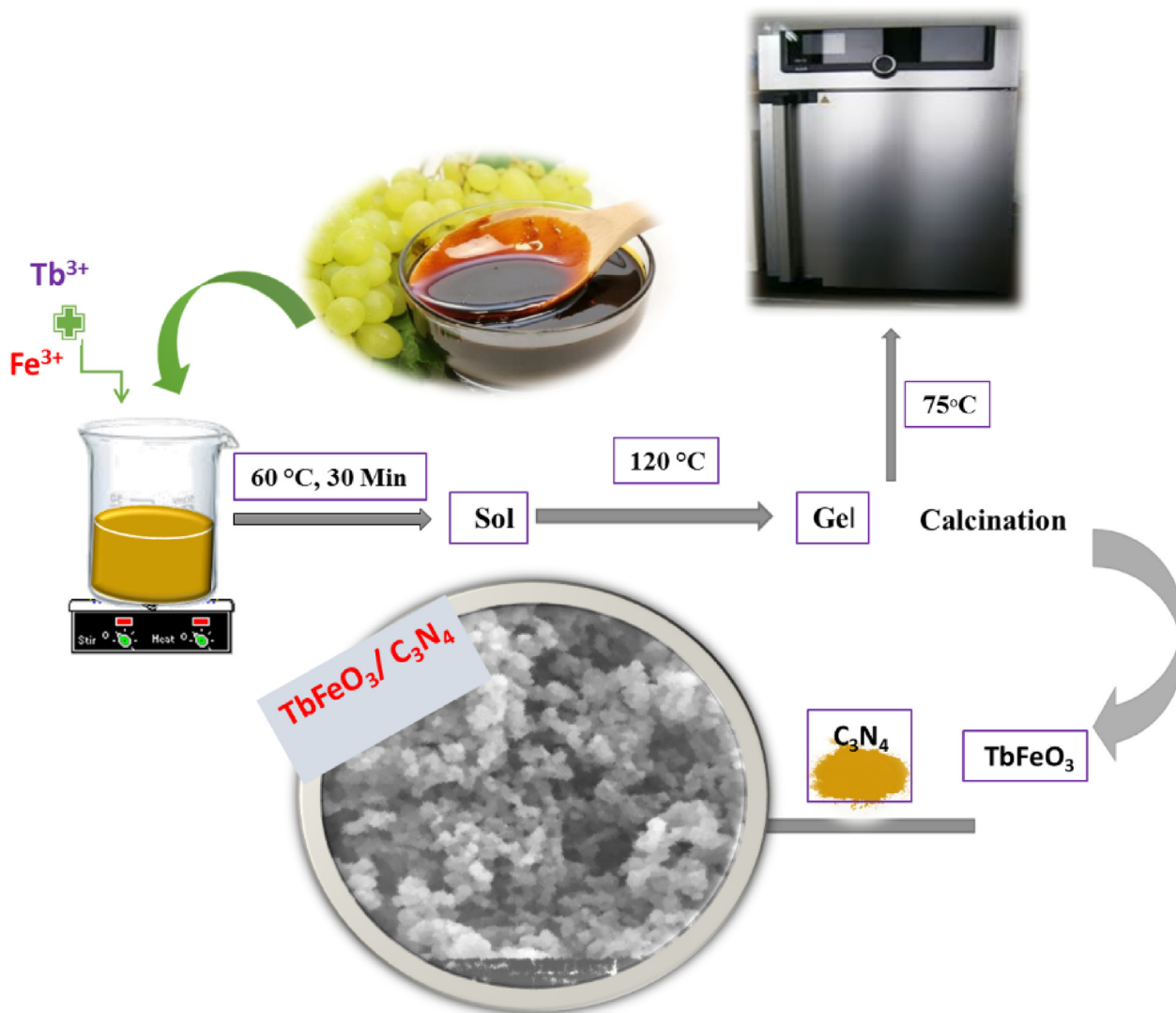
2. Experimental

2.1. Materials and characterization

With the exception of grape extract, all the materials used in this project were readily accessible commercially, and utilized without additional purification. $\text{Fe}(\text{NO}_3)_2 \cdot 9\text{H}_2\text{O}$, and $\text{Tb}(\text{NO}_3)_3 \cdot 6\text{H}_2\text{O}$ with a molecular weight of 251.01, and 453.03 g/mol, respectively, and Melamine with a purity of above 99% were obtained from Merck Co.

2.2. Preparation of grape extract

To prepare grape extract, first, the grapes were washed 2–3 times to be completely clean, then the grape seeds were poured into the blender until the grapes were completely crushed. Then the grape juice was poured into a strainer and the extra skins were removed. At this stage, put a clean cotton cloth on a suitable container and put the grape juice inside the cloth, then



Scheme 1 The formation process of the $\text{tbfeo}_3/\text{g-C}_3\text{N}_4$ nanocrystalline powders by sol-gel auto-combustion method using the Grape Juice as combustion agent.

press until the grape juice is completely smooth and uniform. Then, filtered 100 ml of the prepared fruit juice with Whatman No. 1 and heat it for 2 h at a temperature of 60°C and the obtained thick liquid was kept in the refrigerator.

2.3. Synthesis of pure $TbFeO_3$ and $g-C_3N_4$

In this experiment, $TbFeO_3$ nanostructures were synthesized by sol-gel combustion process (Valian et al., 2022), as follows: (A) 10 mL of water were used to individually dissolve 1 mmol of $Fe(NO_3)_2 \cdot 9H_2O$, and 1 mmol of $Tb(NO_3)_3 \cdot 5H_2O$ (B) The solution was then mixed with 3 mL of grape juice, and heated for 30 min at 60 °C, and after that, at 120 °C, the viscous solution evaporated, and ultimately changed into a gel. (C) The resultant gel was incubated in the oven for 24 h at 75 °C to finish

drying, and the finished powder underwent a 5 h calcination process at 800 °C.

In order to synthesize $g-C_3N_4$ powder, a given amount of Melamine calcined for 4 h at 550 °C.

The synthesis of $TbFeO_3/g-C_3N_4$ nanocrystalline powders using the sol-gel auto-combustion technique with grape juice as the combustion agent is shown in Scheme 1.

2.4. Synthesis of $TbFeO_3/g-C_3N_4$ nanocomposites

A certain quantity of nanoparticles, and 1:1 ratios of $g-C_3N_4$ were first dissolved in water separately, then combined, and put through 5 min of ultrasound (10 s on, 3 s off. With a power of 40 W). It was played on the stereo for 24 h to better homogenize. The finished product was then dried in the oven.

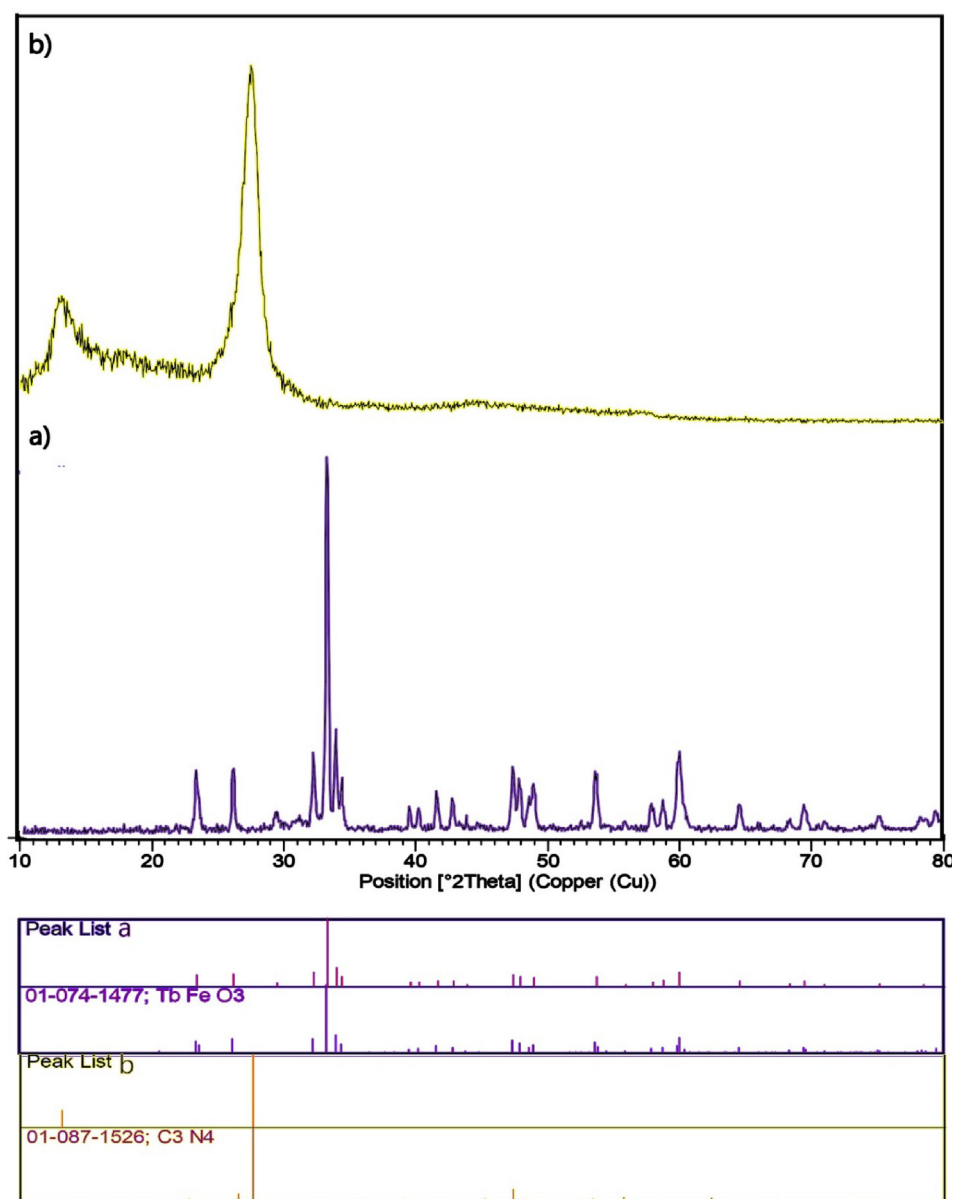


Fig. 1 XRD (a) patterns of the $TbFeO_3$ nanoparticles provided in the presence of Grape Juice at 800 °C, and (b) $g-C_3N_4$ at 550 °C for 4 h.

2.5. Characterization

X-ray diffraction of samples were recorded using XRD-Phillips X'pert PRO with monochromatized Cu-K α radiation ($\lambda = 1.54 \text{ \AA}$). Fourier transform infrared (FTIR) spectroscopy were carried out using Shimadzu IR-460 spectrometer. The surface morphological features of the products were recorded

using a Field Emission Scanning Electron Microscopy (FE-SEM Mira3 Tescan). Energy-dispersive spectroscopy (EDS) analysis was investigated using XL30, Philips microscope. A HT-7700 transmission electron microscope (TEM) operating was used to explore the morphological properties of samples. Vibrating sample magnetometers (VSMs) were used to measure magnetic characteristics (Meghnatis. Daghigh Kavir

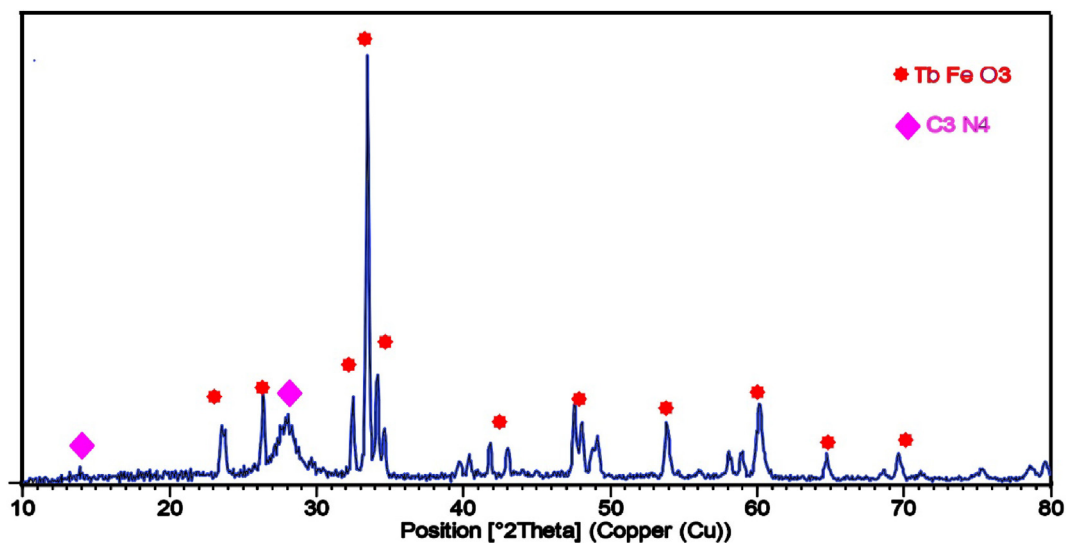


Fig. 2 XRD patterns of the TbFeO₃/g-C₃N₄ nanocomposites.

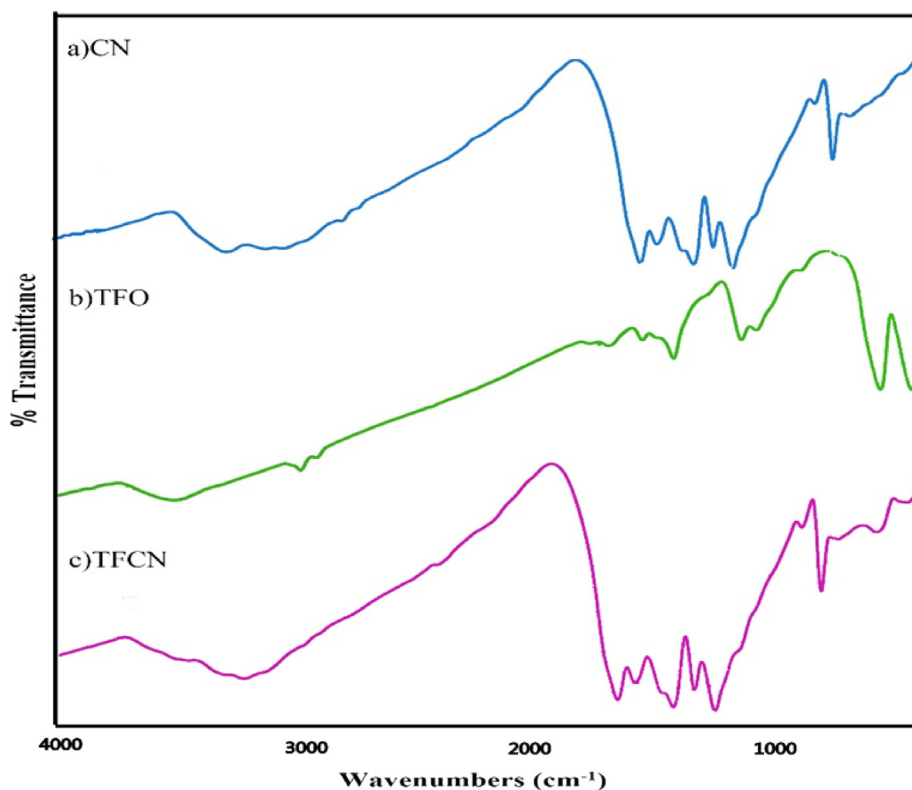


Fig. 3 FTIR spectrum of (a) g-C₃N₄, (b) TbFeO₃, and (c) TbFeO₃/g-C₃N₄ nanocomposites.

Co.; Kashan Kavir; Iran). Using an automated gas adsorption analyzer, the N_2 adsorption/desorption analysis (BET) was carried out at -196°C (Tristar 3000, Micromeritics).A.

2.6. Cell culture and treatment of cells by $TbFeO_3/g-C_3N_4$ nanocomposites

According to earlier reports (Gondo, 2022; Fatahi et al., 2021), the SH-SY5Y, and T98 cell lines were cultured. Glioblastoma cell line T98 is employed in the study of brain cancer, and the

creation of pharmaceuticals. SK-N-SH, a bone marrow biopsy derived line from which SH-SY5Y was cloned, was initially described in 1973 (Biedler et al., 1973). The SH-SY5Y line, which was initially described in 1978, was created from a neuroblast-like subclone of SK-N-SH known as SH-SY. SH-SY5 was then subcloned three times (Biedler et al., 1978). Cloning is simply a form of artificial selection that involves the multiplication of individual cells or a small group of cells that show a certain phenotypic of interest, in this case a feature that is neuron-like. The SH-SY5Y line has two X, and no Y

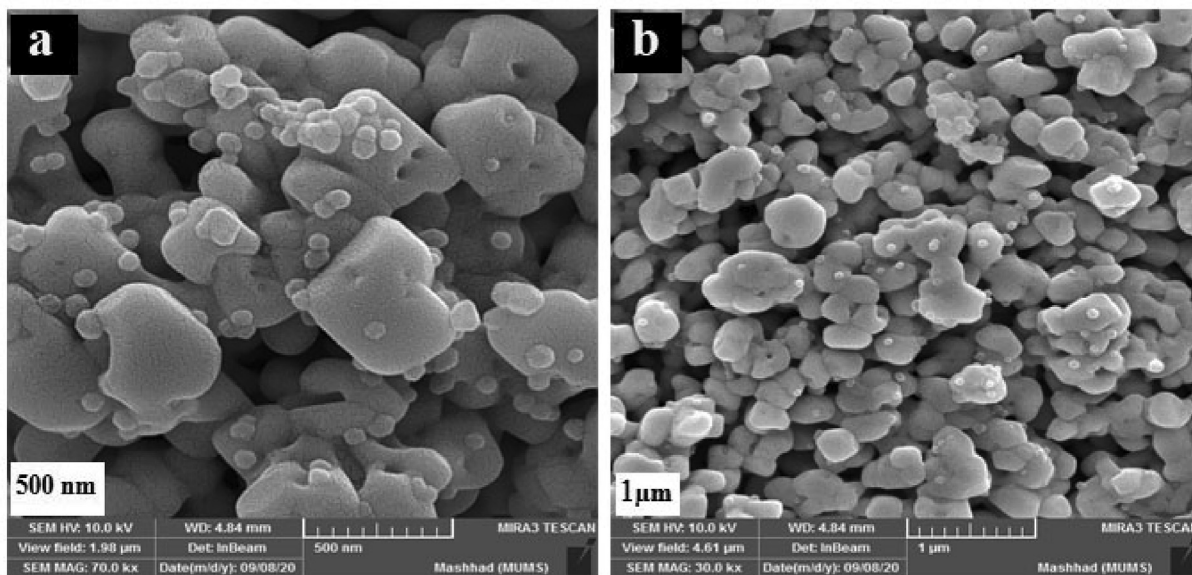


Fig. 4 SEM (a, b) images of the $TbFeO_3$ nanoparticles provided in the presence of Grape Juice as fuel at 800°C for 5 h.

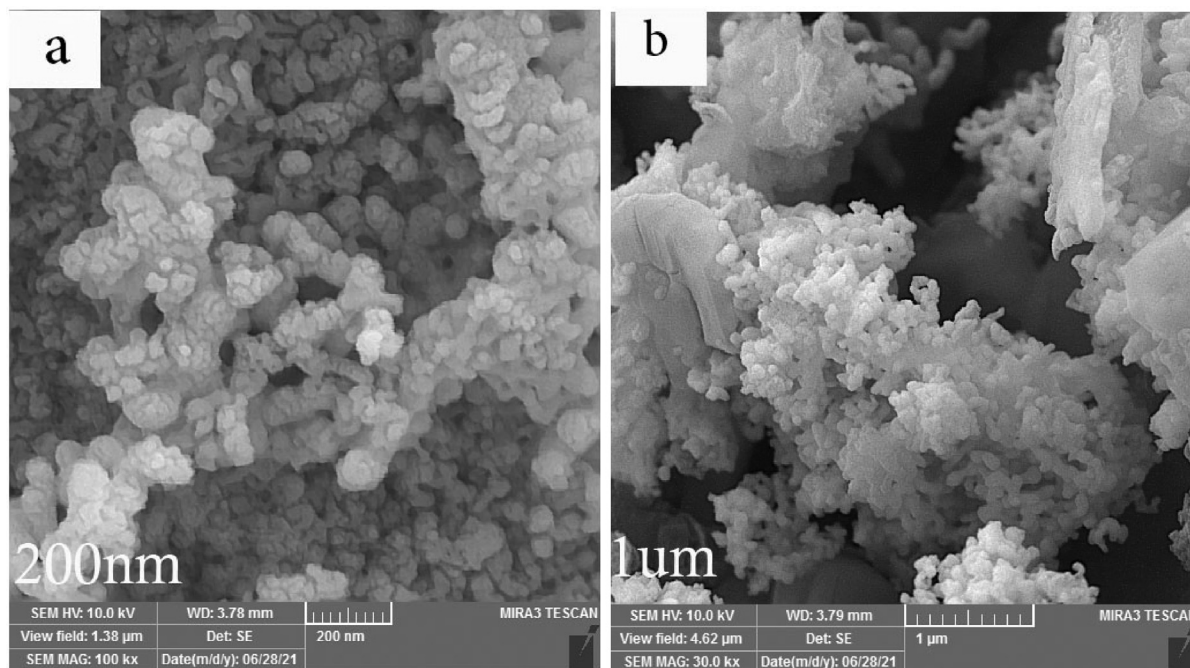


Fig. 5 SEM images of $TbFeO_3/g-C_3N_4$ nanocomposites.

chromosomes, making it genetically female. In a nutshell, Dulbecco's modified Eagle's media (DMEM; Invitrogen Inc. Gibco BRL, Gaithersburg, MD, USA) was used to cultivate human cells from the SH-SY5Y, and T98 lines (Pasteur Institute, Tehran, Iran) in 25 cm² flasks (Iwaki, Tokyo, Japan) at a cell density of 4 × 10⁴ cells/ml. The cultures were maintained at 37 ± 0.5 °C in a humidified environment with 5% CO₂ and supplemented with 1% (v/v) penicillin/streptomycin, and 10% (v/v) fetal calf inactivated serum. Every day, a different media was used. For 24 and 48 h, groups of 4 × 10⁴ cells (for each cell line) were exposed to TbFeO₃/g-C₃N₄ nanocomposites at varying concentrations (0.05–0.8 m/mL). It should be noted that NPs were suspended in DMEM medium, and that, in order to prevent agglomeration before treatment of cells, nanocrystal suspensions were sonicated for 10 min at 40 W. Following each treatment, biochemical, and morphological analyses were carried out.

2.7. Cell viability (MTT Assay)

On the SH-SYY, and T98 cell lines, a cytotoxicity analysis using MTT was performed to evaluate the nanoparticles' biocompatibility. The plates were incubated for 24 h at 37 °C in a CO₂ incubator. Cell lines were planted in 96-well plates at a density of 10 × 10³ cells per well. The plates incubated in a CO₂ incubator at 37 °C/24 h. Following that, various TbFeO₃/g-C₃N₄ nanocomposites suspension concentrations were applied to each well, and they were then incubated for 24, and 48 h. The concentration range shown as 0.05, 0.1, 0.2, 0.4, and 0.8 mg/mL. After adding 10 μL of 5% MTT filtered solution, the medium was replaced with new media, and incubated for 2 h. This equation determines the percentage of viable cells (Amiri et al., 2020); Cell viability (%) = (Atest / Actrl) × 100; where Actrl, and Atest are the control wells, and absorbance values of the test, respectively.

2.8. Statistical analysis

The findings are shown as a mean ± SD; all tests were performed in triplicate. P values under 0.05 are regarded as significant.

3. Results and discussions

3.1. Characterization of the TbFeO₃/g-C₃N₄ nanocomposite

The XRD patterns of (a) g-C₃N₄, and (b) TbFeO₃ nanoparticles obtained at 800 °C for 4 h in the presence of grape juice are shown in Fig. 1. At 2θ = 27.2°, it was observed that g-C₃N₄ exhibited a notable diffraction peak that may be attributed to its (002) facet.

The high crystallinity of TbFeO₃ produced by the sol-gel process was demonstrated by Several pure TbFeO₃ diffraction peaks were seen at 23.2°, 26.06°, 32.14°, 32.18°, 33.8°, 58.6°, and 59.4°. These peaks corresponded closely to the (110), (111), (112), (202), (200), (021), (220), and (004) crystal planes of perovskite-type TbFeO₃ (JCPDS Card No. 47–0068), respectively. The XRD pattern of TbFeO₃/g-C₃N₄ heterojunction nanocomposites samples were shown in Fig. 2, and the diffraction peaks still exhibited the properties of pure TbFeO₃, and g-C₃N₄. Additionally, when the doping ratio of g-C₃N₄ in the samples rose, the peaks about 27.2° progressively grew larger.

The Scherrer's formula can be used to determine the crystallite size as follows: $D_p = 0.9\lambda/\beta\cos\theta$, Where 0.90 is a constant value known as the shape factor, β is the full width at half maximum (FWHM), λ is the wavelength of the X-rays, θ is Bragg's angle, and D_p is the crystallite size. In comparison to pure TbFeO₃ (D_p = 36.44 nm), the size of the TFCN nanocomposite was marginally smaller (38.74 nm) from the

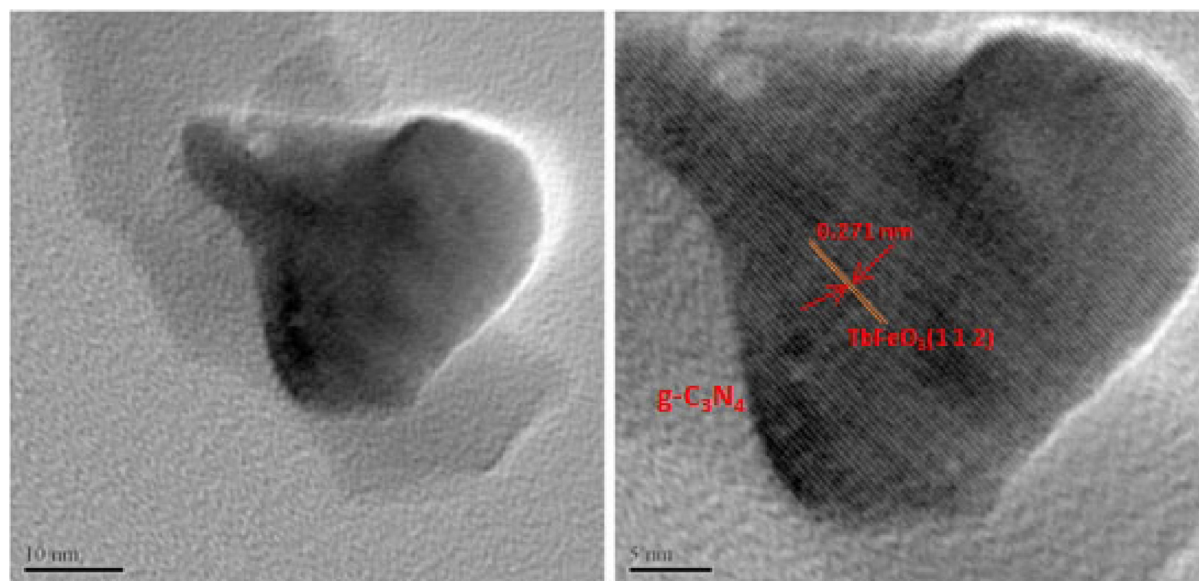


Fig. 6 HR-TEM images of TbFeO₃/g-C₃N₄ nanocomposites.

(112) plane's greatest intensity peak (with Orthorhombic Crystal system), that it could be because of how widely scattered the aggregated TbFeO_3 particles were on the surface of $\text{g-C}_3\text{N}_4$ nanosheets. All of the aforementioned findings supported the development of the connection between $\text{g-C}_3\text{N}_4$, and TbFeO_3 .

Fig. 3(a-c) shows the FTIR spectra of $\text{g-C}_3\text{N}_4$, TbFeO_3 , and a series of $\text{TbFeO}_3/\text{g-C}_3\text{N}_4$ as obtained. Fig. 3b displays the FTIR spectra for the constructed TbFeO_3 nanostructure. The O–H stretching vibrational mode may be the source of the peaks at 3442, and 1621 cm^{-1} . Furthermore, the peaks at 438, and 566 cm^{-1} might be the result of Fe–O stretching vibrations (Yang et al., 2013). Also, when the TbFeO_3 nanostructure was calcined at 800 $^\circ\text{C}$, a faint peak that occurred at 1112 cm^{-1} was attributed to the ambient carbon dioxide.

The conspicuous absorption peak about 3200 cm^{-1} in the spectra of $\text{g-C}_3\text{N}_4$, and $\text{TbFeO}_3/\text{g-C}_3\text{N}_4$ was thought to be caused by the bending, and stretching vibrations of N–H that are caused by the uncondensed terminal amino groups. This

shows that even after heating the urea directly, the products still included amino functionalities. Several prominent peaks in the range of 1200–1650 cm^{-1} were attributed to characteristic $\text{g-C}_3\text{N}_4$'s aromatic heterocycle expansions (Wang et al., 2017; Tian et al., 2018). The distinctive peaks for pure $\text{g-C}_3\text{N}_4$ were compatible with the stretching modes of the CN framework structure of the conjugated aromatic ring at 1294.5, 1435.6, and 1597.2 cm^{-1} . Furthermore, the distinctive absorption peak at 810 cm^{-1} is produced by the breathing vibration of s-triazine for $\text{g-C}_3\text{N}_4$ (Liu et al., 2018).

SEM, and TEM studies were used to evaluate the surface microscopic morphologies of the $\text{g-C}_3\text{N}_4$, TbFeO_3 , and TFCN samples. SEM pictures of the TbFeO_3 nanoparticles are shown in Fig. 4(a, b), which were heated to 800 $^\circ\text{C}$ for 5 h while using grape juice as fuel. Images demonstrate that the pure TbFeO_3 was made up of a large number of grouped spherical nanoparticles. The TbFeO_3 particles were well disseminated and deposited on the surface of $\text{g-C}_3\text{N}_4$ according to the SEM images of Fig. 5(a, b), which also showed that $\text{g-C}_3\text{N}_4$ was stacked by a

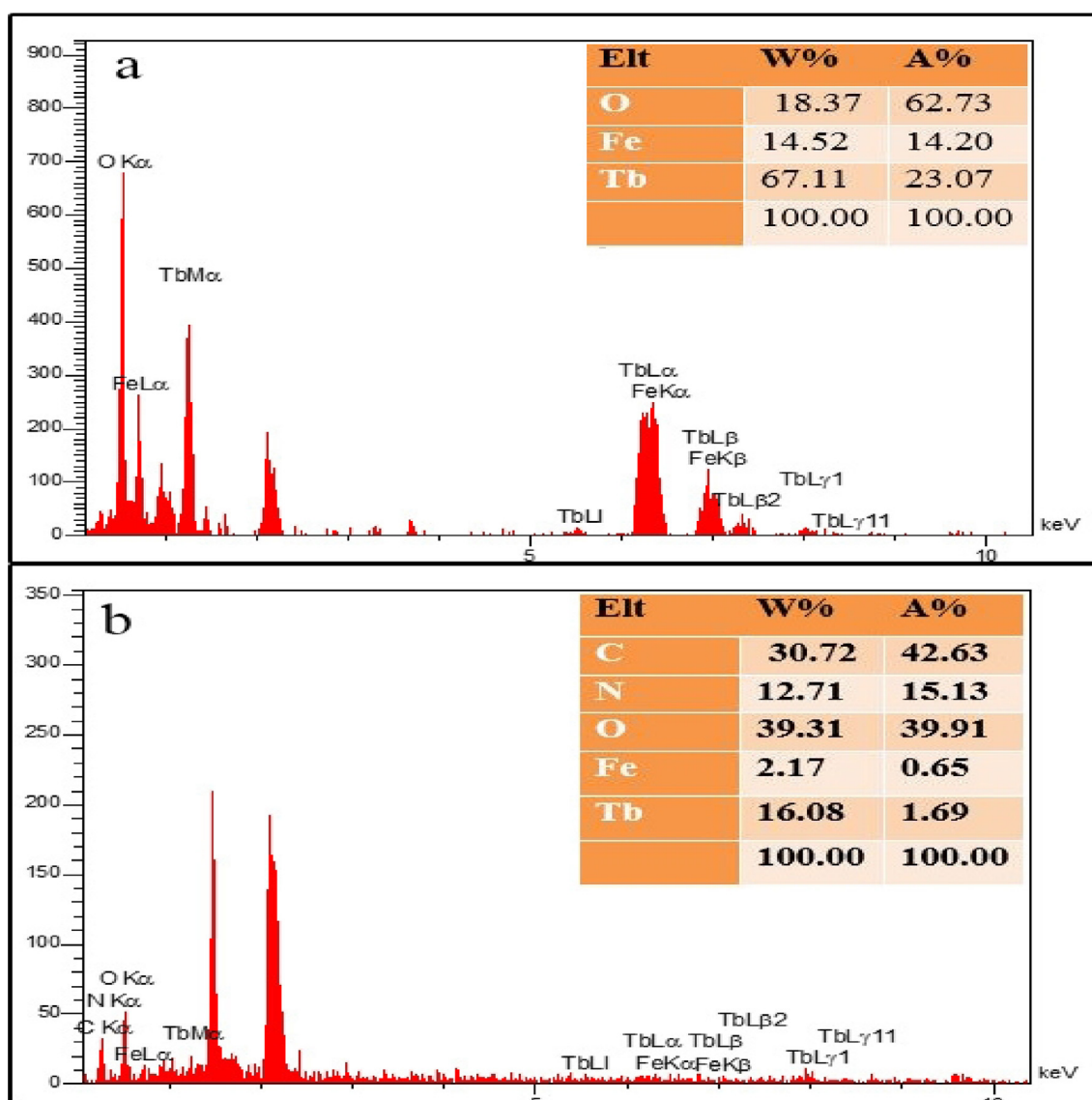


Fig. 7 EDS patterns of, (a) TbFeO_3 and (b) $\text{TbFeO}_3/\text{g-C}_3\text{N}_4$ nanocomposites.

number of irregularly layered nanosheets, and had a significantly larger smooth surface, making it better as a substrate. The nanoparticle size, and internal microstructure of the catalysts as produced were also verified using the HRTEM analysis. The HRTEM of pure TbFeO_3 is shown in Fig. 6. From the images, we could deduce that the TbFeO_3 aggregated particles had sphere-like shapes with a mean diameter of around 30 nm, which was essentially compatible with the calculation result of crystallite size obtained from XRD. Additionally, the TbFeO_3 nanostructure's elemental composition was analyzed using EDS. The EDX of (a) TbFeO_3 , and (b) $\text{g-C}_3\text{N}_4$ nanoplates are shown in Fig. 7. These findings support the inclusion of the elements Fe, O, C, N, and Tb, hence validating the synthesis of the $\text{TbFeO}_3/\text{g-C}_3\text{N}_4$ nanocomposite without the presence of any additional components. Fig. 8 shows the magnetic hysteresis loops of TbFeO_3 when Grape Juice employed for 4 h at a calcination temperature of 800 °C. As a result, we recorded changes in magnetization

against field up to 10,000 Oe at ambient temperature, and the saturation magnetization (M_s) values of the collected samples were around 2.42 emu/g. In reality, the larger cation variations between the two sublattices, and smaller particle sizes in this synthesis method are what primarily contribute to the higher M_s . Then, we discovered fewer coercivity values and a particular magnetic response that could be easily gathered, and changed using an outside magnetic field.

Table 1 Porosity features of synthesized nanomaterials from BET-BJH analyses.

Product	V_m ($\text{cm}^3 \text{g}^{-1}$)	a_s ($\text{m}^2 \text{g}^{-1}$)	Average pore diameter (nm)
TbFeO_3	0.4228	1.8401	23.247
$\text{TbFeO}_3/\text{g-C}_3\text{N}_4$	1.6138	7.0241	32.161

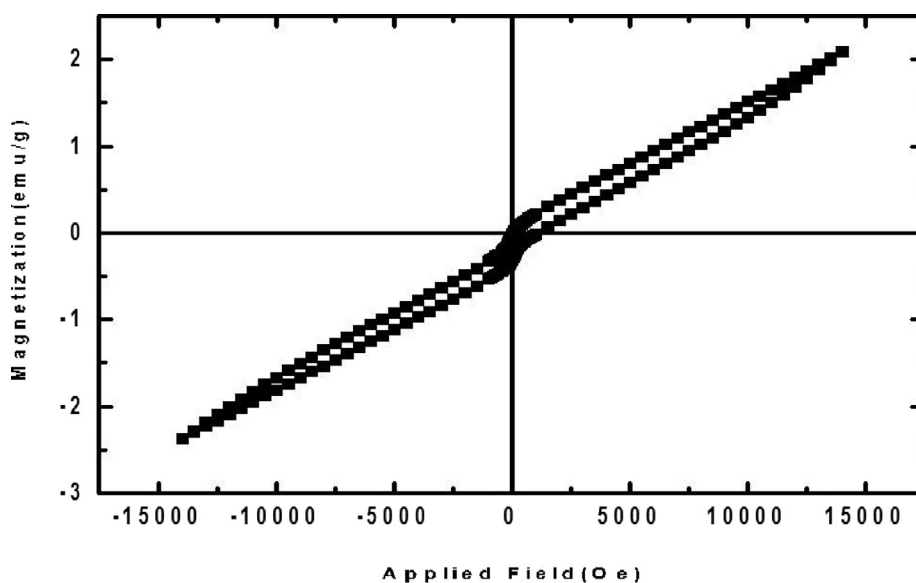


Fig. 8 M- H hysteresis at 300 K for SEM images of the TbFeO_3 nanoparticles provided in the presence of Grape Juice as fuel at 800 °C for 5 h.

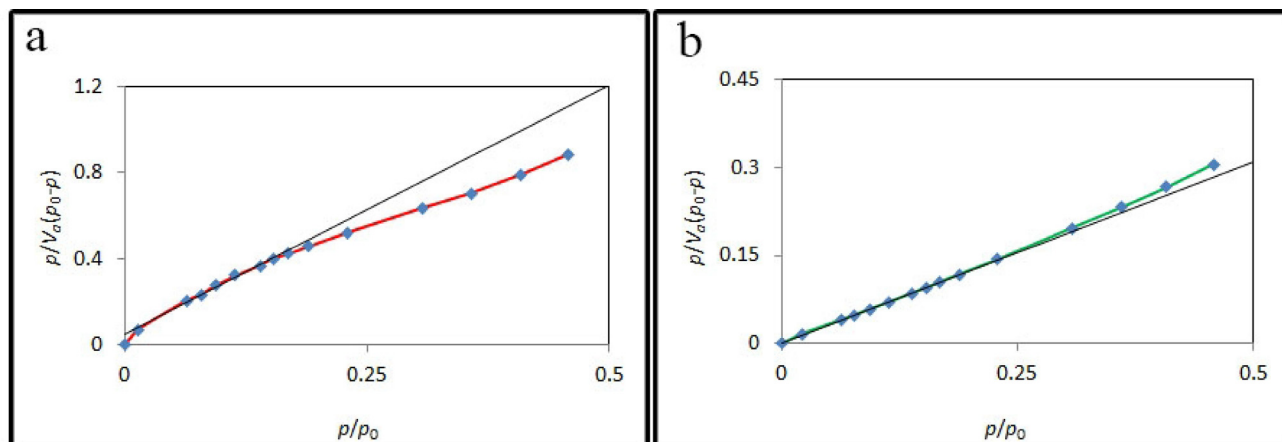


Fig. 9 N_2 adsorption/desorption isotherms and inset image of pore size distribution of $\text{TbFeO}_3/\text{g-C}_3\text{N}_4$ nanocomposites.

Using nitrogen adsorption–desorption tests at 77 K, the specific surface areas, and porous structures of the samples as produced were identified, and the associated curves, and data are displayed in Fig. 9. The N_2 adsorption/desorption isotherms of $TbFeO_3$, and $TbFeO_3/g-C_3N_4$ are illustrated in Fig. 9. This isotherms were categorized as type III according to the IUPAC, the international union of pure and applied chemistry. The compounds that graded for two samples' micropore, and mesopore sizes were given H3-type hysteresis labels. Due to the particular comparative pressure, samples have a wide pore size dispersion from mesopore to micropore (Fig. 9). Table 1 displayed the average pore diameter, total volume, and mediocrity diameter of the nanomaterials.

3.2. Anticancer evaluation of the $TbFeO_3/g-C_3N_4$ nanocomposite

The study and investigation on two cell lines T98 and SH-SY5Y by perovskite nanostructures had not been done until now, except in other works of our team, that in 2023, using nanoparticles $ErFeO_3$, we investigated the survival of cells T98 and SH-SY5Y (Baladi et al., 2023). Also, in 2020, Salawati et al. used molybdenum trioxide nanoparticles to investigate their effect on the survival of glioma and A172 cells. Both T98 and A172 cell lines indicated dose-dependent manner in the presence of increasing concentration of MoO_3 nanostructures, but T98 cells were less sensitive to MoO_3 in comparison

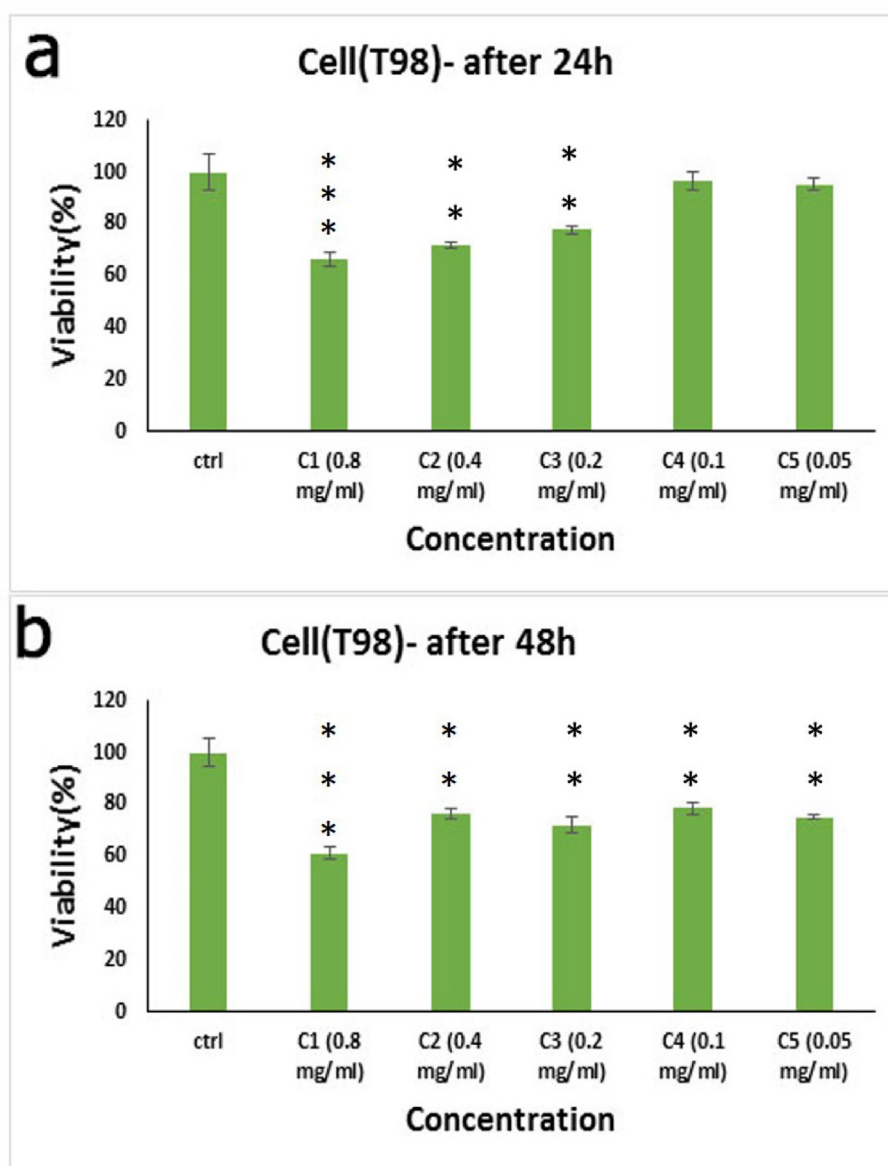


Fig. 10 In vitro cell viability assay, Cell viability of T98 cell lines incubated with $TbFeO_3/g-C_3N_4$ nanocomposites at different concentrations for 24 h (a), and 48 h (b) (SD \pm 2%). Stars indicated significance in compare to control(* $p < 0.05$, ** $p < 0.01$,*** $p < 0.005$).

with A172. Anti-glioma role of MoO₃ nanostructures excited with the aid of UVC illumination studied in vitro. By studying the UV exposure lonely, it was evident that UV effects on cell viability about 50% in both cell lines after 24 h (Masjedi-Arani et al., 2020). in another work also Investigated of toxicity of TiO₂ nanoparticles on glioblastoma and neuroblastoma. The results showed, different concentrations of TiO₂ can be used for different purposes. After administration of 10, 50, 100 and 500 µg/mL TiO₂, 0.043 and 1.4 mW/cm² UVA irradiation, cell viability was investigated after 4, 24 and 48 h by MTT assay (Kazemi et al., 2022).

The anti-cancer effect of TbFeO₃/g-C₃N₄ nanocomposite against T98, and SH-SY5Y cell lines by exposure to NPs at the concentrations of 0.0, 0.05, 0.1, 0.2, 0.4, and 0.8 mg/ml for 24, and 48 h, was determined using MTT assay. The survivability of T98 cell lines exposed to TbFeO₃/g-C₃N₄ nanocomposite at various doses for 24 h (A), and 48 h (B) is shown in Fig. 9 in vitro cell viability experiment.

Viability was noticeably decreased in cultivated cells in the presence of NPs at various doses, suggesting a dose-dependent process. According to Fig. 9, the TbFeO₃/g-C₃N₄ nanocomposite demonstrated a strong index of cytotoxicity impact on malignant cell lines.

The features of glioblastoma may be the cause of the inhibitory effects of NPs on this illness, since these cancer cells have a speedy cell division, greater rate of metabolism, and consequently show improved internalization of NPs, which leads to a higher rate of cell death (Kazemi et al., 2022). With the passage of time, the level of toxicity in different concentrations increases, but the level of toxicity in different doses becomes similar to each other. In total, all the nanoparticles showed similar levels of toxicity to this cell in 24, and 48 h.

The in vitro cell survival experiment was performed on SH-SY5Y cell lines using TbFeO₃/g-C₃N₄ nanocomposite at various doses for 24 h (A), and 48 h (B), and the results are shown

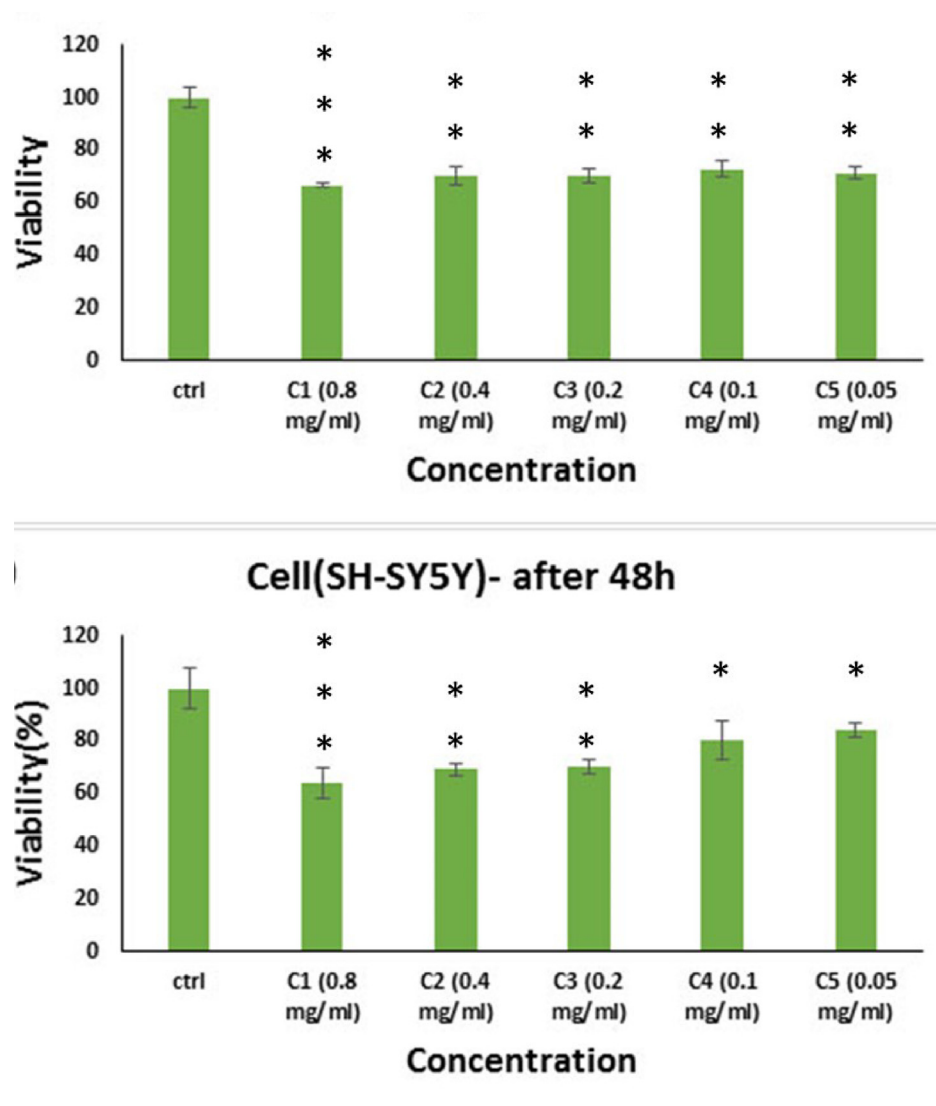


Fig. 11 In vitro cell viability assay, Cell viability of SH-SY5Y cell lines incubated with TbFeO₃/g-C₃N₄ nanocomposites at different concentrations for 24 h (a), and 48 h (b) (SD ± 2%). Stars indicated significance in compare to control(* p < 0.05, ** p < 0.01,*** p < 0.005).

in Fig. 10. In addition to the production of reactive oxygen species, TbFeO₃/g-C₃N₄ nanocomposite also causes a reduction in cellular ATP content and dehydrogenase activity, which causes harm to the mitochondrial respiratory chain and other cellular components and ultimately leads to cell death. Therefore, rather than causing a general disruption in cell membrane functions, phytogetic NPs' cytotoxicity is reliant on the kind of cell that exhibits a unique intracellular mechanism for growth suppression (Fig. 11). Furthermore, the only factors that determine an NP's cytotoxicity are its aggregation state, interaction duration, surface chemistry, shape, and size (Kazemi et al., 2022). Consequently, the toxicity level of all nanoparticles was higher in glioblastoma cells than in neuroblastoma cells.

4. Conclusion

In this study, for the first time a unique, original biosynthetic technique is described in the presence of grape juice, as an environmentally friendly and green precursor, reducing agent, and green capping, using a sol-gel process for the production of uniform, sub-40 nm TbFeO₃/g-C₃N₄ nanocomposites. Since the synthesis of NPs only requires one step, and is non-toxic, simple, affordable, and environmentally benign, it looks to be appropriate for mass manufacturing. The NPs showed a substantial cytotoxic, and dose-dependent impact on the cancer cell lines T98, and SH-SY5Y. In the case of T98 cells, viability was about 60%, 70% and 90% in concentration C1 to C4 respectively after 24 h of drug administration. And viability decreasing by pass the time. Also, viability reduce about 65% in all concentration about SH-SY5Y cells, surprisingly only the first three concentrations, C1 to C3 caused cell death after 48 h of drug administration and in lower concentrations, the death rate should decrease with the passage of time, viability was about 80% and 85% in C4 and C5 respectively. Therefore, In the case of T98 cells, although the concentration of C1 is the most effective. But all concentrations are applicable, according to chemotherapy strategies. Because over time the death rate increases in all concentrations. But in the case of SH-SY5Y cells, only the first three concentrations, C1 to C3 are suitable, because in lower concentrations, the death rate should decrease with the passage of time, and the cell is becoming resistant to the drug. More pharmacological research is undoubtedly required, however the in vitro results showed that TbFeO₃/g-C₃N₄ nanocomposites are promising chemotherapeutic agents against invasive cancer cells, and exhibited high potential for anticancer actions.

CRedit authorship contribution statement

Mahin Baladi: Software, Investigation, Methodology, Writing – original draft, Formal analysis. **Mahnaz Amiri:** Data curation, Software, Writing – review & editing, Writing – original draft. **Maryam Amirinezhad:** Software, Investigation. **Waleed K. Abdulsahib:** Data curation, Software, Writing – review & editing. **Fatemeh Pishgouii:** Formal analysis. **Zahra Golshani:** Formal analysis. **Masoud Salavati-Niasari:** Software, Formal analysis, Methodology, Writing – review & editing, Writing – original draft, Conceptualization, Supervision, Project administration, Investigation, Data curation, Validation, Resources, Visualization.

Declaration of Competing Interest

The authors declare that they have no known competing financial interests or personal relationships that could have appeared to influence the work reported in this paper.

Acknowledgment

The authors are appreciative of the committee of Iran National Science Foundation (INSF, 97017837), and the University of Kashan for financing this research by Grant No (159271/MB3).

References

- T.H. Abdtafweeq, Z.A. Farhan, K. Al-Majdi, M.A. Jawad, R.S. Zabibah, Y. Riadi, S.K. Hadrawi, A. AL-Alwany, M.A. Shams, Ultrasound-Assisted and One-Pot Synthesis of New Fe₃O₄/MOF Magnetic Nano Polymer as a Strong Antimicrobial Agent and Efficient Nanocatalyst in the Multicomponent Synthesis of Novel Pyrano [2, 3-d] pyrimidines Derivatives, *Journal of Inorganic and Organometallic Polymers and Materials*, (2022) 1-12. DOI: 10.1007/s10904-022-02514-7.
- Abdulhusain, Z.H., Mahdi, M.A., Abdulsahib, W.K., Jasim, L.S., 2022. Anabasis articulata exerts an anti-arthritis effect on adjuvant-induced arthritis in rats. *J. Adv. Pharm. Technol. Res.* 13 (4), 276–280. https://doi.org/10.4103/japtr.japtr_440_22.
- Al Alwany, A.A., 2022. Arrhythmia related to hypertensive left ventricular hypertrophy in Iraqi patients: frequency and outcome. *J. Med. Life* 15, 1115. <https://doi.org/10.25122/jml-2022-0214>.
- Amiri, M., Mahmoudi-Moghaddam, H.I., 2021. Green synthesis of ZnO/ZnCo₂O₄ and its application for electrochemical determination of bisphenol A. *Microchem. J.* 160, 105663–110569.
- Amiri, M., Gholami, T., Amiri, O., Pardakhti, A., Ahmadi, M., Akbari, A., Amanatfard, A., Salavati-Niasari, M., 2020. The magnetic inorganic-organic nanocomposite based on ZnFe₂O₄-Imatinib-liposome for biomedical applications, in vivo and in vitro study. *J. Alloy. Compd.* 849, 156604.
- Amiri, M., Khazaeli, P., Salehabadi, A., Salavati-Niasari, M., 2021. Hydrogel beads-based nanocomposites in novel drug delivery platforms: Recent trends and developments. *Adv. Colloid Interface Sci.* 288, 102316.
- Andrei, F., Zăvoianu, R., Marcu, I.-C., 2020. Complex catalytic materials based on the perovskite-type structure for energy and environmental applications. *Materials* 13 (23), 5555.
- M. Ashrafuzzaman, J. Tuszynski, *Membrane-Based Nanotechnology and Drug Delivery, Membrane Biophysics*, Springer 2012, pp. 127-149
- Baladi, M., Amiri, M., Salavati-Niasari, M., 2023. Green sol-gel auto-combustion synthesis, characterization and study of cytotoxicity and anticancer activity of ErFeO₃/Fe₃O₄/rGO nanocomposite. *Arab. J. Chem.* 104575.
- Biedler, J.L., Helson, L., Spengler, B.A., 1973. Morphology and growth, tumorigenicity, and cytogenetics of human neuroblastoma cells in continuous culture. *Cancer Res.* 33 (11), 2643–2652.
- Biedler, J.L., Roffler-Tarlov, S., Schachner, M., Freedman, L.S., 1978. Multiple neurotransmitter synthesis by human neuroblastoma cell lines and clones. *Cancer Res.* 38 (11_Part_1), 3751–3757.
- Bobinov, V., Goroshchenko, S., Rozhchenko, L., Samochernykh, K., Petrov, A., 2021. Historical aspects of microsurgical treatment of brain aneurysms. *History Med.* 7, 179–188. <https://doi.org/10.17720/2409-5834.v7.2.2021.08h>.
- Chen, S., Kang, Z., Zhang, X., Xie, J., Wang, H., Shao, W., Zheng, X., Yan, W., Pan, B., Xie, Y., 2017. Highly active Fe sites in ultrathin pyrrhotite Fe₇S₈ nanosheets realizing efficient electrocatalytic oxygen evolution. *ACS Cent. Sci.* 3 (11), 1221–1227.
- Chen, X., Zhang, M., Qin, H., Zhou, J., Shen, Q., Wang, K., Chen, W., Liu, M., Li, N., 2022. Synergy effect between adsorption and heterogeneous photo-Fenton-like catalysis on LaFeO₃/lignin-biochar composites for high efficiency degradation of ofloxacin under visible light. *Sep. Purif. Technol.* 280, 119751.

- Dai, J., Song, J., Qiu, Y., Wei, J., Hong, Z., Li, L., Yang, H., 2019. Gold nanoparticle-decorated g-C₃N₄ nanosheets for controlled generation of reactive oxygen species upon 670 nm laser illumination. *ACS Appl. Mater. Interfaces* 11 (11), 10589–10596.
- N. Farooq, A. ur Rehman, A.M. Qureshi, Z. ur Rehman, A. Ahmad, M.K. Aslam, H.M.A. Javed, S. Hussain, M.A. Habila, N. AlMasoud, Au@ GO@ g-C₃N₄ and Fe₂O₃ nanocomposite for efficient photocatalytic and electrochemical applications, *Surfaces and Interfaces* 26 (2021) 101399
- Fatahi, A., Soleimani, N., Afrough, P., 2021. Anticancer activity of kefir on glioblastoma cancer cell as a new treatment. *Int. J. Food Sci.* 2021.
- Fei, B., Tang, Y., Wang, X., Dong, X., Liang, J., Fei, X., Xu, L., Song, Y., Zhang, F., 2018. One-pot synthesis of porous g-C₃N₄ nanomaterials with different morphologies and their superior photocatalytic performance. *Mater. Res. Bull.* 102, 209–217.
- Goel, P., Sundriyal, S., Shrivastav, V., Mishra, S., Dubal, D.P., Kim, K.-H., Deep, A., 2021. Perovskite materials as superior and powerful platforms for energy conversion and storage applications. *Nano Energy* 80, 105552.
- Gondo, H.K., 2022. Effect of isotiocyanate therapy on trophoblast cell culture hyperglycemia atmosphere in apoptosis, caspase-3, NO, VEGF. *History Med.* 8, 62–67. <https://doi.org/10.17720/2409-5834.v8.1.2022.008>.
- Goudarzi, M., Salavati-Niasari, M., Amiri, M., 2019. Effective induction of death in breast cancer cells with magnetite NiCo₂O₄/NiO nanocomposite. *Compos. B Eng.* 166, 457–463.
- Grossman, J.H., McNeil, S.E., 2012. Nanotechnology in cancer medicine. *Phys. Today* 65 (8), 38.
- Guo, H., Zhou, X., Zhang, Y., Yao, Q., Qian, Y., Chu, H., Chen, J., 2020. Carbamazepine degradation by heterogeneous activation of peroxymonosulfate with lanthanum cobaltite perovskite: performance, mechanism and toxicity. *J. Environ. Sci.* 91, 10–21.
- Huang, Y., He, S., Cao, W., Cai, K., Liang, X.-J., 2012. Biomedical nanomaterials for imaging-guided cancer therapy. *Nanoscale* 4 (20), 6135–6149.
- Hussein, B.Y., Mohammed, A.M., 2021. Green synthesis of ZnO nanoparticles in grape extract: their application as anti-cancer and anti-bacterial. *Mater. Today: Proc.* 42, A18–A26.
- Kazemi, F., Esmaceli, M., Mohammadzadehjehani, P., Amiri, M., Vosough, P., Ahmadi-Zeidabadi, M., 2022. Investigation of toxicity of TiO₂ nanoparticles on glioblastoma and neuroblastoma as the most widely used nanoparticles in photocatalytic processes. *Environ. Health Eng. Manage. J.* 9 (4), 365–374.
- Kudarha, R.R., Sawant, K.K., 2017. Albumin based versatile multifunctional nanocarriers for cancer therapy: fabrication, surface modification, multimodal therapeutics and imaging approaches. *Mater. Sci. Eng. C* 81, 607–626.
- L. Li, F. Wang, J. Feng, S. Guo, M. Xu, L. Wang, G. Quan, Direct Z-scheme GdFeO₃/g-C₃N₄ heterostructures with outstanding photocatalytic activity, (2021).
- Ling, D., Hackett, M.J., Hyeon, T., 2014. Surface ligands in synthesis, modification, assembly and biomedical applications of nanoparticles. *Nano Today* 9 (4), 457–477.
- Liu, Z., Hadi, M.A., Aljuboory, D.S., Ali, F.A., Jawad, M.A., Ameen, A.-A., Hadrawi, S.K., Mundher, T., Riadi, Y., Amer, R.F., 2022. High efficiency of Ag⁰ decorated Cu₂MoO₄ nanoparticles for heterogeneous photocatalytic activation, bactericidal system, and detection of glucose from blood sample. *J. Photochem. Photobiol. B Biol.* 236. <https://doi.org/10.1016/j.jphotobiol.2022.112571>
- Liu, J.-L., Jiang, J., Zhang, J.-Q., Chai, Y.-Q., Xiao, Q., Yuan, R., 2020. The combination of ternary electrochemiluminescence system of g-C₃N₄ nanosheet/TEA/Cu@ Cu₂O and G-quadruplex-driven regeneration strategy for ultrasensitive bioanalysis. *Biosens. Bioelectron.* 152, 112006.
- Liu, E., Jin, C., Xu, C., Fan, J., Hu, X., 2018. Facile strategy to fabricate Ni₂P/g-C₃N₄ heterojunction with excellent photocatalytic hydrogen evolution activity. *Int. J. Hydrogen Energy* 43 (46), 21355–21364.
- Lokapur, V., Jayakar, V., Divakar, M., Chalannavar, R.K., Lasrado, L., Shantaram, M., 2022. ZnO nanoparticles with spectroscopically controlled morphology, bioinspired from *Hologarna grahamii* (Wight) Kurz and delving its antioxidant and anticancer potential on A498 cell line. *Mater. Today Commun.* 31, 103338.
- Mahde, B.W., Sultan, A.M., Mahdi, M.A., Jasim, L.S., 2022. Kinetic adsorption and release study of sulfadiazine hydrochloride drug from aqueous solutions on GO/P(AA-AM-MCC) composite. *Int. J. Drug Deliv. Technol.* 12 (4), 1583–1589. <https://doi.org/10.25258/ijddt.12.4.17>.
- Majid, A., Tunney, J., Argue, S., Wang, D., Post, M., Margeson, J., 2005. Preparation of SrFeO_x 2.85 perovskite using a citric acid assisted Pechini-type method. *J. Alloy. Compd.* 398 (1–2), 48–54.
- Masjedi-Arani, M., Amiri, M., Amiri, O., Ahmadi, M., Salavati-Niasari, M., 2020. Glioma cells eradication by photoexcitation of bioengineered molybdenum trioxide nanoparticles synthesized by wet chemical and microwave route: dose dependent photosensitizer bioactivity. *Int. J. Pharm.* 591, 120021.
- Maurya, D., Thota, H., Nalwa, K.S., Garg, A., 2009. BiFeO₃ ceramics synthesized by mechanical activation assisted versus conventional solid-state-reaction process: a comparative study. *J. Alloy. Compd.* 477 (1–2), 780–784.
- Montaseri, H., Kruger, C.A., Abrahamse, H., 2020. Recent advances in porphyrin-based inorganic nanoparticles for cancer treatment. *Int. J. Mol. Sci.* 21 (9), 3358.
- Narducci, D., 2007. An introduction to nanotechnologies: what's in for us? *Vet. Res. Commun.* 31 (1), 131–137.
- Ordás, I., Mould, D.R., Feagan, B.G., Sandborn, W.J., 2012. Anti-TNF monoclonal antibodies in inflammatory bowel disease: pharmacokinetics-based dosing paradigms. *Clin. Pharmacol. Ther.* 91 (4), 635–646.
- Qi, F., Zhao, L., Zhou, A., Zhang, B., Li, A., Wang, Z., Han, J., 2015. The advantages of using traditional Chinese medicine as an adjunctive therapy in the whole course of cancer treatment instead of only terminal stage of cancer. *Biosci. Trends* 9 (1), 16–34.
- Rezaeifar, M., Mahmoudvand, H., Amiri, M., 2016. Formulation and evaluation of diphenhydramine gel using different gelling agents. *Pharm. Chem.* 8 (5), 243–249.
- Shamim, M., Perveen, M., Nazir, S., Hussain, M., Mehmood, R., Khan, M.I., Iqbal, J., 2021. DFT study of therapeutic potential of graphitic carbon nitride (g-C₃N₄) as a new drug delivery system for carboplatin to treat cancer. *J. Mol. Liq.* 331, 115607.
- Tian, J., Zhang, L., Wang, M., Jin, X., Zhou, Y., Liu, J., Shi, J., 2018. Remarkably enhanced H₂ evolution activity of oxidized graphitic carbon nitride by an extremely facile K₂CO₃-activation approach. *Appl. Catal. B: Environ.* 232, 322–329.
- L.A. Torre, F. Bray, R.L. Siegel, J. Ferlay, J. Lortet-Tieulent, A. Jemal, Global cancer statistics, 2012, CA: a cancer journal for clinicians 65(2) (2015) 87-108.
- Valian, M., Salavati-Niasari, M., Ganduh, S.H., Abdulsahib, W.K., Mahdi, M.A., Jasim, L.S., 2022. Sol-gel auto-combustion synthesis of a novel chitosan/Ho₂Ti₂O₇ nanocomposite and its characterization for photocatalytic degradation of organic pollutant in wastewater under visible illumination. *Int. J. Hydrogen Energy* 47 (49), 21146–21159.
- Varandili, S.B., Babaei, A., Ataie, A., 2018. Characterization of B site codoped LaFeO₃ nanoparticles prepared via co-precipitation route. *Rare Met.* 37 (3), 181–190.
- Wang, Z.L., 2004. Zinc oxide nanostructures: growth, properties and applications. *J. Phys. Condens. Matter* 16 (25), R829.
- Wang, W., An, T., Li, G., Xia, D., Zhao, H., Jimmy, C.Y., Wong, P. K., 2017. Earth-abundant Ni₂P/g-C₃N₄ lamellar nanohybrids for

- enhanced photocatalytic hydrogen evolution and bacterial inactivation under visible light irradiation. *Appl. Catal. B: Environ.* 217, 570–580.
- Wang, X., Blechert, S., Antonietti, M., 2012. Polymeric graphitic carbon nitride for heterogeneous photocatalysis. *ACS Catal.* 2 (8), 1596–1606.
- Wang, A., Wang, C., Fu, L., Wong-Ng, W., Lan, Y., 2017. Recent advances of graphitic carbon nitride-based structures and applications in catalyst, sensing, imaging, and LEDs. *Nano-Micro Lett.* 9 (4), 1–21.
- Yadav, A.R., Mohite, S.K., 2020. Carbon nanotubes as an effective solution for cancer therapy. *Res. J. Pharma. Dosage Forms Technol.* 12 (4), 301–307.
- Yang, G., Phua, S.Z.F., Bindra, A.K., Zhao, Y., 2019. Degradability and clearance of inorganic nanoparticles for biomedical applications. *Adv. Mater.* 31 (10), 1805730.
- Yang, H., Zhang, J., Lin, G., Xian, T., Jiang, J., 2013. Preparation, characterization and photocatalytic properties of terbium orthoferrite nanopowder. *Adv. Powder Technol.* 24 (1), 242–245.
- Ye, C., Wang, R., Wang, H., Jiang, F., 2020. The high photocatalytic efficiency and stability of LaNiO₃/gC₃N₄ heterojunction nanocomposites for photocatalytic water splitting to hydrogen. *BMC Chem.* 14 (1), 1–13.
- Yu, W.-D., Sun, G., Li, J., Xu, J., Wang, X., 2019. Mechanisms and therapeutic potentials of cancer immunotherapy in combination with radiotherapy and/or chemotherapy. *Cancer Lett.* 452, 66–70.
- Zhang, G., Lin, L., Li, G., Zhang, Y., Savateev, A., Zafeiratos, S., Wang, X., Antonietti, M., 2018. Ionothermal synthesis of triazine–heptazine-based copolymers with apparent quantum yields of 60% at 420 nm for solar hydrogen production from “Sea Water”. *Angew. Chem. Int. Ed.* 57 (30), 9372–9376.
- Zhang, X., Xie, X., Wang, H., Zhang, J., Pan, B., Xie, Y., 2013. Enhanced photoresponsive ultrathin graphitic-phase C₃N₄ nanosheets for bioimaging. *J. Am. Chem. Soc.* 135 (1), 18–21.
- Zhang, Z., Yang, X., Zhang, Y., Zeng, B., Wang, S., Zhu, T., Roden, R.B., Chen, Y., Yang, R., 2006. Delivery of telomerase reverse transcriptase small interfering RNA in complex with positively charged single-walled carbon nanotubes suppresses tumor growth. *Clin. Cancer Res.* 12 (16), 4933–4939.
- Zhao, F., Li, Z., Wang, L., Hu, C., Zhang, Z., Li, C., Qu, L., 2015. Supramolecular quantum dots as biodegradable nano-probes for upconversion-enabled bioimaging. *Chem. Commun.* 51 (67), 13201–13204.
- D. Zheng, J. Zhou, Z. Fang, T. Heil, A. Savateev, Y. Zhang, M. Antonietti, G. Zhang, X. Wang, H 2 and CH 4 production from bio-alcohols using condensed poly (heptazine imide) with visible light, *Journal of Materials Chemistry A* (2021).
- M. Zia, S. Gul, J. Akhtar, I.u. Haq, B.H. Abbasi, A. Hussain, S. Naz, M.F. Chaudhary, Green synthesis of silver nanoparticles from grape and tomato juices and evaluation of biological activities, *IET nanobiotechnology* 11(2) (2017) 193-199